International Symposium
On Turbulence and Shear Flow
Phenomena (TSFP-8)
August 28 - 30, 2013 Poitiers, France

QUANTIFYING UNCERTAINTIES IN TURBULENT FLOW SIMULATIONS

Gianluca Iaccarino and Michael Emory

Department of Mechanical Engineeing
Institure for Computational Mathematical Engineering
Stanford University
Bldg 500, RM 500-I, Stanford CA 94305 - USA
jops@stanford.edu

ABSTRACT

The Reynolds averaged Navier-Stokes equations represent an attractive alternative to direct numerical simulation of turbulence due to their simplicity and reduced computational expense. In the literature it is well established that structure of Reynolds averaged turbulence models are fundamentally limited in their ability to represent the turbulent processes - introducing epistemic *model-form* uncertainty into the predictions. Sensitivity analysis and probabilistic approaches have been used to address these uncertainties, however there is no well established framework within the turbulence modeling community to quantify this important source of error. This work introduces a new approach for addressing epistemic uncertainty which is then demonstrated for the ow over a 2D transonic bump configuration. The well known SST k-ω turbulence model is considered. The reported quantities are the wall pressure, separation location, and reattachment location along the bottom wall of the domain. The results show the new method is able to introduce bounding behavior on the numerical and experimental predictions for these quantities.

INTRODUCTION

Computational fluid dynamics (CFD) is widely used by engineers in a range of applications, providing a wealth of information about the flow characteristics. Despite this ability to produce comprehensive and detailed information, engineering performance is typically measured using only few predicted values, for example maximum temperature or drag coefficient . These parameters require accurate characterization and are critical for effective design. These predicted quantities of interest (QOI) are often very sensitive, making the proper characterization of the underlying physics important for reliable and safe product design.

Directly solving the Navier-Stokes equations, which govern the behavior of fluid motions, is largely intractable for many problems of interest. The large separation of spatial and temporal scales for complex flows renders the computational cost of these simulations unaffordable. A simplified set of governing equations, the Reynolds averaged Navier-Stokes (RANS) equations, are typically solved although they require additional relations (turbulence models) to close the problem.

Reynolds averaged models maintain a wide spread use because of their limited computational expense and ease-of-use. The main criticism is their structural inability to represent fundamental turbulence processes – for example the energy transfer within the inertial range – and therefore, the lack of universality in their formulation. Turbulence modelers and practitioners typically resort to tuning and calibration to experimental datasets to improve the prediction capability of specific closures, thus using the models merely as sophisticated interpolations.1 These simplified physical models introduce epistemic *model-form* uncertainty into simulations, and to date there is no well established framework to quantify its effect on the resulting predictions.

A **fundamentally new approach** is required to objectively assess the ability of turbulence models to credibly estimate quantities of interest in engineering flows. The present work represents a first step towards the creation of error models to identify and characterize inaccuracy in the physical assumptions used, borrowing ideas from error estimates in numerical analysis. The driving principle is that, in general terms, it is easier to define bounds for a quantity instead of characterizing it precisely: bounds can be based on theoretical reasoning or fundamental properties and can be defined even without a detailed knowledge of the underlying physical process. The introduction of bounds as opposed to precise statements is the main new component in this proposal and obviously goes well beyond the characterization of turbulence. The traditional approach to modeling is based on the idea of approximation: *say where the answer is, and then try to minimize the bias*. The present approach of bounding is exactly the opposite: *say where you know the answer is not and then try to tighten the range*.

In the present context, we start by identifying the basic hypotheses used in the model formulation and to construct local sensors based on computable quantities to track their validity: in the absence of violations the computations must be considered valid. On the other hand, the identification of flow conditions not consistent with the initial assumptions must trigger the injection of uncertainty. These will negatively affect the confidence in the end results.

The article is organized as follows: section II illustrates the basic idea and section III describes the transonic bump flow being investigated and compares a standard RANS computation with the experimental results. Section IV discusses the uncertainties inherent to turbulence modeling and

motivates a novel frame- work for addressing model-form uncertainty. Finally section V develops the new methodology and compares the results to the experiment and nominal RANS computations.

METHODOLOGY

Consider the classical example of the prediction of aerodynamic loads on a transonic airfoil. The application of conventional turbulence models will likely lead to the situation illustrated in Fig. 1, where three different models were used. These simulations do not provide any explicit information on the accuracy of the models, and the results are typically interpreted using previous experience on a subjective basis. It is worth noting that the three models reported in Fig. 1 do not bound the actual solution and the results might be incorrectly biased.

Our objective is not to develop a new turbulence closure, but to revisit the limitations of well-established RANS models, and to evaluate if they operate outside the intended range of applicability. As a simple introductory example, it is well known that eddy viscosity models for high speed flows are inaccurate in predicting the turbulence amplification across shock waves.3 New models have been proposed to address this limitation,4 typically by introducing additional hypotheses and altering the behavior of the original model. In the present context, it is quite simple to detect the region(s) where the turbulence production rate might be erroneous (shock detection is fairly straightforward) and therefore define the sensor: this is schematically illustrated in Fig. 2.

As per the determination of the applicability bounds of turbulent production it is logical to consider the shear-induced production as an upper limit to the actual turbulence generation.4 The lower bound can be assumed to be no production. At this point a *turbulence-production-error sensor* can be formulated and used in actual computations. The presence of a shock wave will activate the sensor and the uncertainty introduced locally will be propagated through the computation. This will lead to potential uncertainty in the output quantity of interest (as illustrated in Fig. 2).

The impact of the inaccuracy in the assumption of the turbulence/shock interaction might be very small, and, therefore, in spite of a clear limitation of the original model, our confidence in the predictions should remain high. On the other hand, an unacceptably low degree of confidence (very large error bars in Fig. 2) will provide rationale for improving the definition of the bounds or for the adoption of a more sophisticated closure.

RANS modeling

Almost all RANS closures are constructed to estimate the Reynolds stress tensor R_{ij}, defined as $\overline{u_i'u_j'}$ or $\widetilde{u_i''u_j''}$ for incompressible and compressible flow, respectively, with the appropriate use of Reynolds or Favre decompositions $u_i = \overline{u}_i + u_i' = \widetilde{u}_i + u_i''$. Most engineering models rely on the eddy-viscosity hypothesis that assumes that the stress R_{ij} is linearly related to the mean rate-of-strain S_{ij} through a scalar eddy-viscosity ν_t, i.e.,

$$R_{ij}^{\mathrm{ev}} = \frac{2k}{3}\delta_{ij} - 2\nu_t S_{ij}^{\mathrm{dev}}, \qquad (1)$$

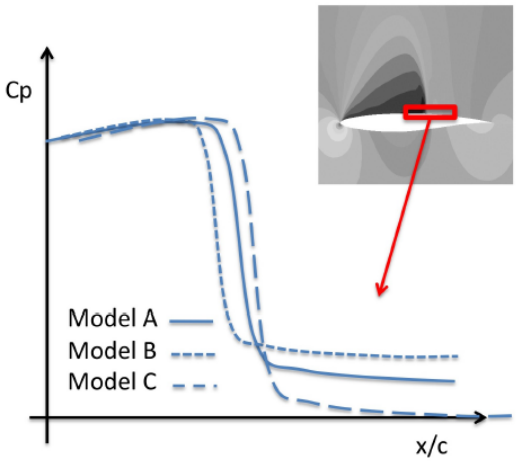

Figure 1. Pressure distribution on a transonic airfoil. Three Reynolds Averaged models are used to predict the interaction between the boundary layer and the shock on the upper surface of the airfoil. Remark: there is no guarantee that the three predictions bound the actual true solution!

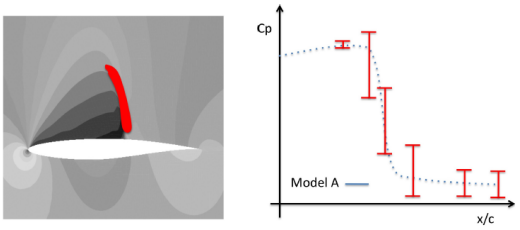

Figure 2. (Left) A shock-detection sensor identifies a region where the model assumptions might be invalid; in this case the turbulence production/dissipation across a shock wave. (Right) Bounds for the corresponding physical process are defined and uncertainty is injected locally leading to error bounds on the predictions.

where S_{ij}^{dev} is the deviatoric (trace-free) part of the strain-rate tensor $S_{ij} = (\partial_j\widetilde{u}_i + \partial_i\widetilde{u}_j)/2$. The superscript "ev" denotes that this assumed stress-strain relationship in Eq. (1) is used only in eddy-viscosity models, including mixing-length models (where k is neglected) as well as one-, two- and three-equation models such as, for example, the Spalart-Allmaras, $k-\omega$, and V2F models. These models differ in how they compute k and ν_t, for example, in the commonly used $k-\omega$ model transport equations are solved for k and ω and then $\nu_t = C_\nu k/\omega$. These transport equations include model coefficients that are typically specified by matching known asymptotic behaviors, e.g. the decay of isotropic turbulence [6].

Eddy viscosity models rely on two modeling *layers*: the hypothesized stress-strain relationship in Eq. (1) and the equations assumed to represent the terms therein. Thus, there are multiple potential sources of errors and it has been traditionally very difficult to identify the dominant cause of discrepancies in complex problems. It is worth mentioning that in addition to coefficients used in the models, e.g. C_ν in the $k-\omega$ model, the transport equations and the stress-strain hypothesis imply a functional relationship that it is not valid in general. For example, in steady state flows, the turbulent kinetic energy production typically balances dissipation and

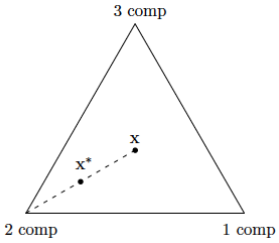

Figure 3. Barycentric map: illustration showing how the state x given by the base-model is perturbed towards the limiting state of two-component turbulence.

both these processes require modeling.

While much past work on UQ of RANS models has focused on characterizing the sensitivity of the predictions to the model coefficients [7, 8], this approach neglects any errors introduced in the physical assumption used to construct the assumed model-form, such as Eq. (1).

In the present work we take the opposite approach: we focus directly on the hypothesized stress-strain relationship in Eq. (1) and inject uncertainty directly into it to quantify if there is any fundamental bias induced in the predictions. The underlying RANS model that produces estimates of k and ν_t, and thus through Eq. (1) R_{ij}, is viewed as a black box, merely returning the Reynolds stress as a function of the velocity field $\overline{u}_i$ or $\widetilde{u}_i$ (for Reynolds and Favre-averaged equations, respectively).

It is important to note that if we view a RANS model as producing an estimate R_{ij}, then the whole UQ machinery and ideas presented below apply to any RANS model, including those not based on the eddy-viscosity assumption.

R_{ij} decomposition

The focus of the present work is to model the uncertainty in the predicted R_{ij}, in a way agnostic to the RANS model used. To this end, it is useful to decompose the modeled Reynolds stress into factors determining its amplitude, shape, and orientation [9]. This is done by introducing the anisotropy tensor a_{ij} as

$$a_{ij} = \frac{R_{ij}}{2k} - \frac{1}{3}\delta_{ij}\,.$$

Realizability of the Reynolds stress [10] requires that $a_{ij} \in [-2/3, 4/3]$ for $i = j$ and that $a_{ij} \in [-1, 1]$ for $i \neq j$. Furthermore, an eigen-decomposition of the (symmetric trace-free) anisotropy tensor yields

$$a_{ik}v_{kl} = v_{ik}\Lambda_{kl}\,,$$

where v_{ij} is the matrix of orthonormal eigenvectors and Λ_{kl} is the diagonal matrix of eigenvalues λ_l satisfying $\lambda_1 + \lambda_2 + \lambda_3 = 0$. Multiplication of v_{jl} from the right yields $a_{ij} = v_{ik}\Lambda_{kl}v_{jl}$ and thus the Reynolds stress produced by the RANS model can be decomposed as

$$R_{ij} = 2k\left(\frac{1}{3}\delta_{ij} + v_{ik}\Lambda_{kl}v_{jl}\right)\,. \tag{2}$$

Note that the amplitude, shape, and orientation of the tensor are directly controlled by k, the eigenvalues λ_i, and the eigenvectors v_{ij}, respectively.

The eigen-decomposition of a_{ij} is useful to separate the shape and the orientation of the Reynolds stress tensor from each other, but also to directly enforce the realizability constraints on a_{ij} through the barycentric map [11]. Consider an equilateral triangle in two dimensions defined by the three corners $\mathbf{x}_{1c}$, $\mathbf{x}_{2c}$ and $\mathbf{x}_{3c}$, where $\mathbf{x} = (x, y)$ is the coordinate in this space. Then $\mathbf{x} = \mathbf{x}_{1c}(\lambda_1 - \lambda_2) + \mathbf{x}_{2c}(2\lambda_2 - 2\lambda_3) + \mathbf{x}_{3c}(3\lambda_3 + 1)$ defines a linear mapping between the three eigenvalues λ_l and the coordinates $\mathbf{x}$. This mapping, together with the requirement that the sum of the eigenvalues is zero, is an invertible one-to-one mapping $\mathbf{x} = B\lambda$.

Perturbed R^*_{ij}

To model errors in the underlying RANS model perturbations are injected into the decomposed Reynolds stress defined in Eq. (2). Thus

$$R^*_{ij} = 2k^*\left(\frac{1}{3}\delta_{ij} + v^*_{ik}\Lambda^*_{kl}v^*_{jl}\right)\,, \tag{3}$$

where $k^* = k + \Delta k$ is the perturbed turbulence kinetic energy and Λ^*_{kl} is the diagonal matrix of perturbed eigenvalues λ^*_l. The perturbed eigenvector matrix is defined as $v^*_{ij} = q_{ik}v_{kj}$ where q_{ik} is an orthonormal rotation matrix. Note that there are 6 degrees-of-freedom in these perturbations: one for the amplitude, two for the shape (since the sum of the eigenvalues is zero), and three for the orientation (since the eigenvectors are orthonormal). The perturbed eigenvalues are defined implicitly through the coordinates in the barycentric map. In other words, $\lambda^*_l = B^{-1}\mathbf{x}^*$ with the perturbation defined in the barycentric map.

There is an implied spatial variation in these perturbations. Most obviously, there is no reason to believe that Δk should be constant in space; it is much more reasonable to suppose that the Δk error in the turbulence model is strongly varying in space, but with a spatial dependency clearly connected to the modeling assumptions and the underlying flow structures. For example, errors in the Reynolds stresses computed in attached boundary layer are likely to be strongly correlated to the wall distance.

For the eigenvalues determining the shape of the Reynolds stress tensor, the perturbation has both a magnitude (the distance $|\mathbf{x}^* - \mathbf{x}|$) and a direction within the barycentric map, both of which could vary in space. The issue of how to specify the spatial variation of these perturbations (amplitudes, directions, etc) is very important, but not discussed in detail in the present manuscript. The focus here is on presenting the general *uncertainty injection* framework and on applying it to simple test cases in which it is quite simple to identify where the modeling assumptions might be incorrect. The further objective of the present work is to illustrate how the injected uncertainties have physical meaning and interpretations, and also to show how this injection affects and *envelopes* the predictions.

As part of this objective, we consider perturbations in the barycentric map in only three directions: towards each of the three corners of the triangle $\mathbf{x}_{1c}$, $\mathbf{x}_{2c}$ and $\mathbf{x}_{3c}$, representing the limiting states of one-, two- and three-component (isotropic) turbulence. The perturbations are defined through the distance δ of movement towards the target corner. Thus the perturbed location in the barycentric map is $\mathbf{x}^* = \mathbf{x} + \delta(\mathbf{x}_t - \mathbf{x})$, where subscript t denotes the target state, illustrated in Fig. 3 for $\mathbf{x}_t = \mathbf{x}_{2c}$ and $\delta = 0.5$. With the linear map B, we have the perturbed eigenvalues $\lambda^* = B^{-1}\mathbf{x}^* = (1-\delta)B^{-1}\mathbf{x} + \delta B^{-1}\mathbf{x}_t = (1-\delta)\lambda +$

Figure 4. Pressure contours of the nominal condition Delery transonic bump

$\delta B^{-1}\mathbf{x}_t$. Taking the three corners $\mathbf{x}_{1c}$, $\mathbf{x}_{2c}$ and $\mathbf{x}_{3c}$ as the target states, we have $B^{-1}\mathbf{x}_{1c} = (2/3,-1/3,-1/3)^T$, $B^{-1}\mathbf{x}_{2c} = (1/6,1/6,-1/3)^T$ and $B^{-1}\mathbf{x}_{3c} = (0,0,0)^T$.

It is instructive to investigate how the perturbation of the shape of the Reynolds stress tensor, i.e., the eigenvalues or the position in the barycentric map, affect the actual Reynolds stress. If we consider no perturbations on the amplitude or orientation (i.e., $k^* = k$ and $v^*_{ij} = v_{ij}$), then the anisotropic (or deviatoric) part of the perturbed Reynolds stress in Eq. (3) becomes

$$\begin{aligned} R^{*,\mathrm{dev}}_{ij} &= 2kv_{ik}\left[(1-\delta)\Lambda_{kl} + \delta\Lambda^{(t)}_{kl}\right]v_{jl} \\ &= (1-\delta)R^{\mathrm{dev}}_{ij} + \delta\, 2k\, v_{ik}\Lambda^{(t)}_{kl}v_{jl}\,, \end{aligned} \tag{4}$$

where $\Lambda^{(t)}_{kl}$ is the diagonal matrix of the three target eigenvalue states $B^{-1}\mathbf{x}_t$. Perturbations towards the three-component (isotropic) state simply reduce the modeled shear stresses proportionally to δ, i.e. they represent a bias towards lower shear stress.

DELERY BUMP

To test the framework in a more physically complex case (transonic flow, shock-boundary layer interaction, streamline curvature, separation) we investigate Delery's Case C [22]. Calculations are performed on a mesh containing 280 x 100 elements in the streamwise and wall-normal directions, respectively, and the near-wall grid is designed to give y^+ of order 1 for the first line of cells. The computational domain extends upstream of the start of the bump (Fig. 4) so that a uniform inflow condition is used and boundary layers develop along the walls. The extent upstream is specified so the boundary layer at the start of the bump geometry coincides with the experimental boundary layer height at this location. Adiabatic wall boundaries are applied along the top and bottom of the domain, while symmetry conditions are used in the spanwise directions.

The distribution of Mach number over the bump is reported in Fig. 4. The inflow conditions correspond to $M = 0.6$ and the flow becomes supersonic ($M = 1.4$) over the bump, forming a curved shock bridging the entire channel. This in turns leads to a strong interaction between the shock and the bottom wall boundary layer, creating a distinctive lambda shock structure and a separation bubble at the foot of the bump.

The computations are carried out using the baseline SST closure and perturbations towards the three corners of the barycentric maps for different combinations of amplitude (δ) and marker. As in the duct problem both the whole domain and wall-distance based markers are used. A $d_c = 0.006$m is used for the wall-distance marker, chosen because this is the height of the bottom wall separation bubble in the baseline solution. The results are summarized in Fig. 6 in terms of pressure and shear stress distributions on the lower wall. The results once again confirm the general

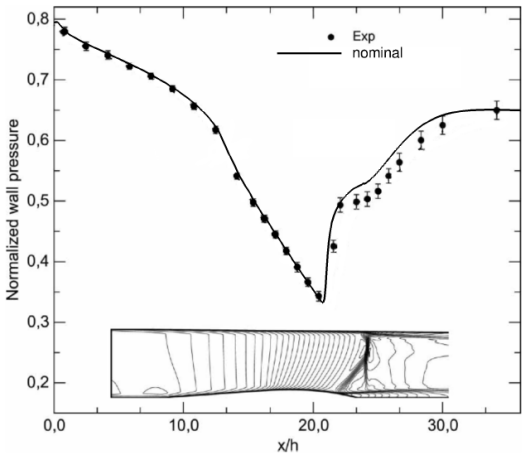

Figure 5. Wall pressure profile with experimental data (symbols) and the nominal RANS computation (line). The inset image shows Mach number contours.

enveloping behavior and sensitivity to the choice of marker, although qualitatively the different choices (uniform versus wall-distance based) lead to similar results.

More quantitative results are extracted by analyzing the length of the separation bubble and how it is affected by the different markers. In Fig. 7 the streamlines are reported while the actual location of the separation and the extent of the bubble are presented in Table 1.

The perturbations towards $\mathbf{x}_{1c}$ and $\mathbf{x}_{2c}$ bias the solution towards a smaller separation-bubble by biasing the Reynolds stress tensor towards states with higher shear stress.

CONCLUSIONS

Uncertainty quantification of Reynolds-averaged Navier-Stokes closures is tackled using a physics-based perturbation approach that aims at enveloping the predictions, thus leading to an estimate of the confidence in the predictions. The physics-based UQ approach has two main components: identification of regions in the flow where the modeling assumptions are plausibly inaccurate, followed by injection of physically meaningful and realizable perturbations to the modeled Reynolds stress tensor in those regions. The present manuscript is focused solely on the second of these components. Specifically, an eigen-decomposition of the Reynolds stress is used to allow for independent perturbations of the magnitude, anisotropy and direction of the Reynolds stress tensor. Moreover, the barycentric map is used to define the perturbations to the anisotropy of the stress. In addition to ensuring a physically realizable perturbed stress, this approach also ensures that the perturbations have physical meaning and interpretations.

Results are presented for incompressible flow in a turbulent channel and duct and for the transonic flow over a curved bump. The computations illustrate the ability of the present methodology to provide envelopes around the baseline model predictions. Of particular importance is the study of the duct flow in which secondary flows are generated solely by the turbulence anisotropy and therefore not predicted by the original eddy-viscosity closure. The proposed perturbation framework is capable of generating secondary recirculation. The secondary flow is physically re-

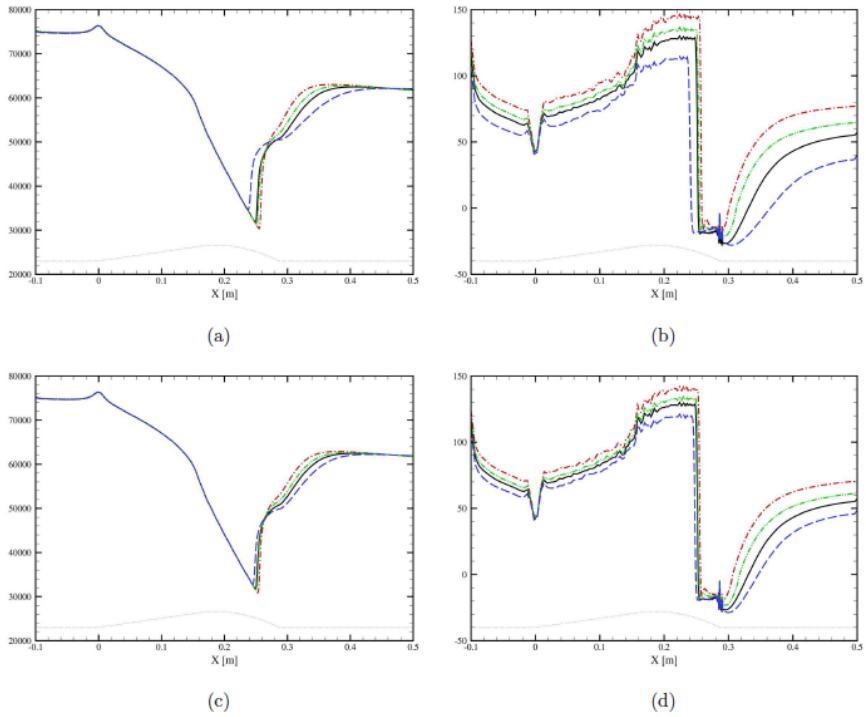

Figure 6. (Color online) Delery bump: profiles of P_w (left column) and τ_w (rigt column) along the bottom wall, geometry depicted by the dotted line. The baseline solution is the solid line, and perturbations towards $\mathbf{x}_{1c}$ are represented by the dash-dot line (red online), $\mathbf{x}_{2c}$ by the dash-dot-dot (green online), and $\mathbf{x}_{3c}$ by the dashed line (blue online). All perturbations use $\delta_{max} = 0.5$ for the different markers: whole domain (top row) and $d_c = 0.006$m (bottom row).

Table 1. Separation location x_s and separation bubble length ($l_{bubble} = x_r - x_s$) along the bottom wall for the various Delery simulations. When the 'whole domain' marker is used $\delta = \delta_{max}$.

Simulation		x_s [m]		l_{bubble} [mm]	
SST baseline		0.252		78.01	
δ_{max}		whole domain	d_c = 0.006 [m]	whole domain	d_c = 0.006 [m]
$\mathbf{x}_{1c}$	0.1	0.254	0.253	62.80	67.70
	0.25	0.256	0.254	52.05	59.09
	0.5	0.258	0.256	42.23	49.93
	1.0	0.260	0.258	34.36	40.48
$\mathbf{x}_{2c}$	0.1	0.253	0.253	71.20	73.77
	0.25	0.253	0.253	64.48	68.59
	0.5	0.254	0.254	57.24	63.30
	1.0	0.256	0.255	46.66	54.52
$\mathbf{x}_{3c}$	0.1	0.251	0.252	83.68	81.24
	0.25	0.249	0.251	95.47	86.39
	0.5	0.242	0.249	122.65	97.22
	1.0	0.207	0.241	91.53	132.64

alistic when perturbing towards the two-component limit, which is the correct physical limit when approaching a solid wall. Interestingly, a completely unphysical "reverse" secondary flow is generated when perturbing towards the one-component limit.

The proposed approach for uncertainty injection needs to be combined with a methodology to determine where (in space) the model should be trusted or not. Simply put,

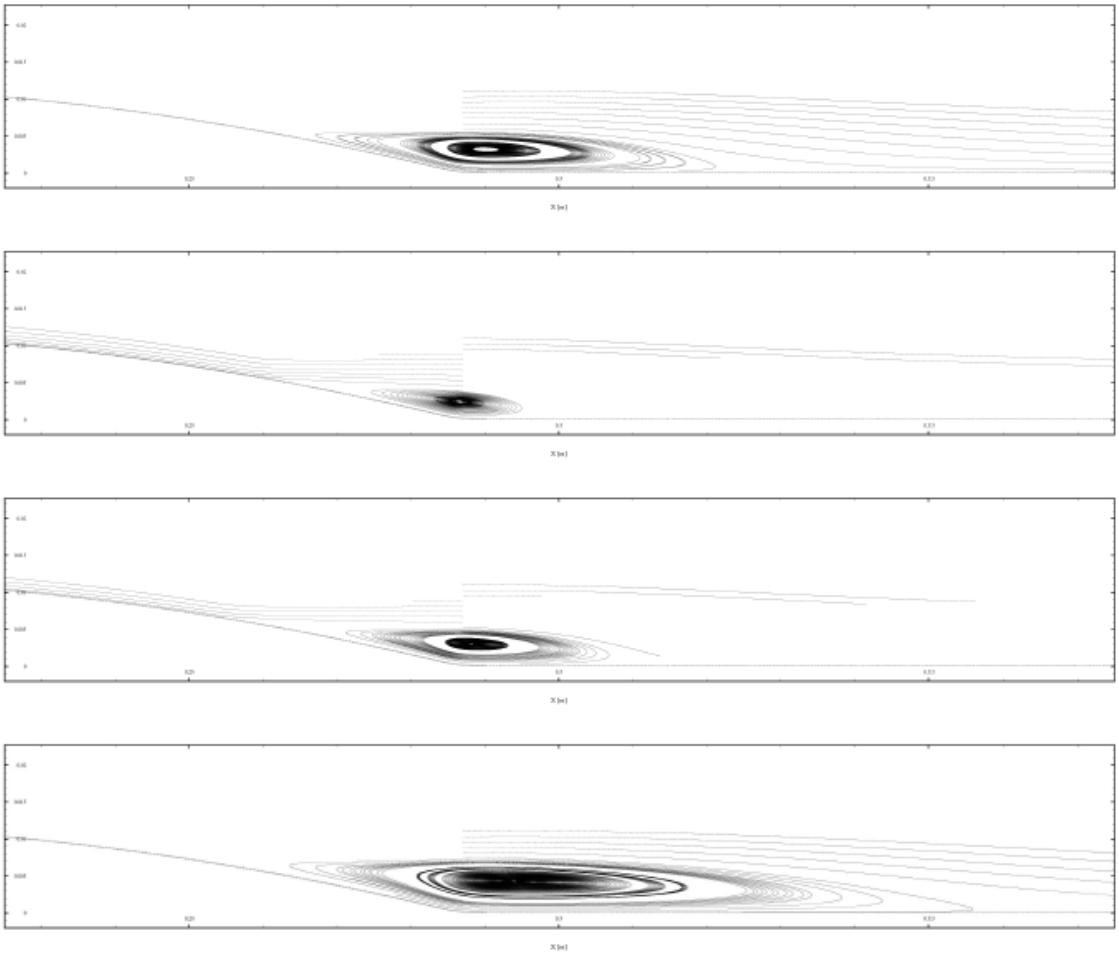

Figure 7. Delery bump: streamlines depicting the separation bubble located along the bottom wall at the end of the bump, geometry depicted by the dotted line. From top to bottom are the baseline, $\mathbf{x}_{1c}$, $\mathbf{x}_{2c}$, and $\mathbf{x}_{3c}$ perturbation solutions at $\delta = 0.5$, using the whole domain marker.

it would be much too pessimistic to assume that a well-validated RANS model is wrong *everywhere* in the domain. Instead, it is much more realistic to assume that the model is correct in those regions where the flow is similar to what the model was designed and validated for (e.g., attached boundary layers), and that the model is erroneous in other, more complex, flow-regions. The development of such a *marker* function that identifies these different regions is part of ongoing work.

Acknowledgments

This research was supported by the Department of Energy [National Nuclear Security Administration] under award number NA28614.

REFERENCES

[1] A. Raftery, T. Gneiting, F. Balabdaoui, and M. Polakowski, "Using Bayesian Model Averaging to Calibrate Forecast Ensembles,". Mon. Wea. Rev., **133**, 1155 (2005).

[2] T. Oliver and R. Moser, "Bayesian uncertainty quantification applied to RANS turbulence models," 13^{th} *European Turbulence Conference*, 2011.

[3] S. Cheung, T. Oliver, E. Prudencio, S. Prudhomme, and R. Moser, "Bayesian uncertainty analysis with applications to turbulence modeling", Reliability Engineering and System Safety **96**, 1137 (2011).

[4] G. Iaccarino, R. Pecnik, J. Glimm, and D. Sharp, "A QMU Approach for Characterizing the Operability Limits of Air-Breathing Hypersonic Vehicles", Reliability Engineering and System Safety, **96** No. 9, 1150 (2010).

[5] G. Iaccarino, D. Sharp, and J. Glimm, "Quantification of Margins and Uncertainties using Multiple Gates and Conditional Probabilities", Reliability Engineering and System Safety, (to be published).

[6] D. Wilcox, *Turbulence Modleing for CFD* (DCW Industries, Inc, 1993).

[7] P. Platteeuw, G. Loeven, and H. Bijl, "Uncertainty Quantification Applied to the k-ε Model of Turbulence Using the Probabilistic Collocation Method," 49^{th} *AIAA Structures, Structural Dynamics, and Materials Conference*, 2008, pp. 1–17.

[8] M. Dunn, B. Shotorban, and A. Frendi, "Uncertainty Quantification of Turbulence Model Coefficients via Latin Hypercube Sampling Method," Journal of Fluids Engineering **133**, 1 (2011).

[9] L. Terentiev, "The Turbulence Closure Model Based on Linear Anisotropy Invariant Analysis," Ph.D. Thesis, Universität Erlangen-Nürnberg, 2006.

[10] C. Speziale, R. Abid, and P. Durbin, "On The Realizability of Reynolds Stress Turbulence Closures," Journal of Scientific Computing **9**, 369 (1994).

[11] S. Banerjee, R. Krahl, F. Durst, and C. Zenger, "Presentation of anisotropy properties of turbulence, invariants versus eigenvalue approaches," J. of Turbulence **8**, 1 (2007).

[12] R. Pecnik, V. Terrapon, F. Ham, G. Iaccarino, and H. Pitsch, "Reynolds-Averaged Navier-Stokes Simulations of the HyShot II Scramjet," AIAA Journal **50**, No. 8, 1717 (2012).

[13] E. Toro, *Riemann solvers and numerical methods for fluid dynamics: a practical introduction* (Springer, 1st ed., 1999).

[14] J. Mandal and J. Subramanian, "On the link between weighted least-squares and limiters used in higher-order reconstructions for finite volume computations of hyperbolic equations," Applied Numerical Mathematics **58**, 705 (2001).

[15] R. Pecnik, V. Terrapon, F. Ham, and G. Iaccarino, "Full system scramjet simulation," *Center for Turbulence Research Annual Research Briefs*, 2009, pp. 33–45.

[16] V. Venkatakrishnan, "Convergence to steady state solutions of the euler equations on unstructred grids with limiter," *Journal of Computational Physics*, **118**, 120 (1995).

[17] T. Barth and D. Jespersen, "The design and application of upwind schemes on unstructured meshes," AIAA Paper No. 1989–0366, 1989.

[18] F. Menter, "Two-equation eddy-viscosity turbulence models for engineering applications," AIAA Journal **32**, No. 8, 1598 (1994).

[19] S. Hoyas and J. Jimenez, "Scaling of the velocity uctuations in turbulent channels up to Re = 2003," Phys. Fluids **18**, 2006.

[20] K. Lien, J. Monty, M. Chong, and A. Ooi, "The Entrance Length for Fully Developed Turbulet Channel Flow," *15th Australian Fluid Mechanics Conference*, 2004.

[21] R. Pecnik and G. Iaccarino, "Predictions of turbulent secondary flows using the $v^2 - f$ model," AIAA Paper No. 2008-3852, 2008.

[22] J. Delery, "Investigation of Strong Shock Turbulent Boundary Layer Ineraction in 2-D Transonic Flows with Emphasis on Turbulence Phenomena," AIAA Paper No. 1981-1245, 1981.